Spin-torch experiment on reaction centers of Rhodobacter sphaeroides

Sai Sankar Gupta, K.B.

Chapter 2

Two-dimensional nanosecond laser-flash photo-CIDNP MAS NMR experiments provide direct access to the electronic structure of the donor in bacterial reaction centers

Abstract

Although the two branches of cofactors are apparently symmetrically arranged, electron transfer in photosynthetic reaction centers (RCs) of the photosynthetic purple bacteria *Rhodobacter (R.) sphaeroides* wildtype (WT) occurs exclusively via the redox chain formed by the cofactors on the A branch. Previous ^{13}C and ^{15}N photochemically induced dynamic nuclear polarization (photo-CIDNP) solid-state magic-angle spinning (MAS) NMR studies using selective isotope labelling patterns of the cofactors have shown that an electron distribution map of the ground state can be obtained. Here we present a complete mapping of the electronic ground state of the donor cofactors in RCs (WT). Following biosynthetic labelling of RCs from *R. sphaeroides* (WT), the increased selectivity of the novel time-resolved two-dimensional dipolar-assisted rotational resonance (DARR) MAS NMR experiment simplifies the signal assignment compared to complex spectra of the same RCs obtained by continuous illumination. The shielding pattern of the ^{13}C nuclei confirms that there is excess electron density towards pyrrole ring III of $P_{L^{\cdot}}$ compared with pyrrole ring III of P_M and the pattern of ^{13}C shifts for the ring carbons is well in line with $P_L^{\delta-}P_M^{\varepsilon-}$ charge transfer character, with $\delta > \varepsilon$. Hence symmetry breaking of the electronic structure with excess negative charge on the P_L is detected in the ground state, to mediate asymmetric electron transfer following excitation.

2.1 Introduction

The discovery of the solid-state photo-CIDNP (photochemically induced dynamic nuclear polarization) effect (for reviews, (Jeschke & Matysik, 2003; Daviso *et al.*, 2008b)) by Zysmilich and McDermott in frozen and quinone-blocked bacterial reaction centers (RCs) of *Rhodobacter (R.) sphaeroides* R26 by ^{15}N magic-angle spinning (MAS) NMR under continuous illumination with white light offers NMR access to the electron-nuclear processes during charge separation (Zysmilich & McDermott, 1994). By induction of a non-Boltzmann nuclear spin polarization upon photo-reaction in rigid samples, a signal enhancement of a factor of more than 10,000 has been observed by ^{13}C MAS NMR in several RCs (Prakash *et al.*, 2005; Prakash *et al.*, 2006; Roy *et al.*, 2008). The solid-state photo-CIDNP effect can now be produced routinely for the enhancement of the ^{13}C MAS NMR for various photosynthetic RCs, including those of the purple bacteria of *R. sphaeroides* wild type (WT) (Prakash *et al.*, 2005) and R26 (Zysmilich & McDermott, 1994; Prakash *et*

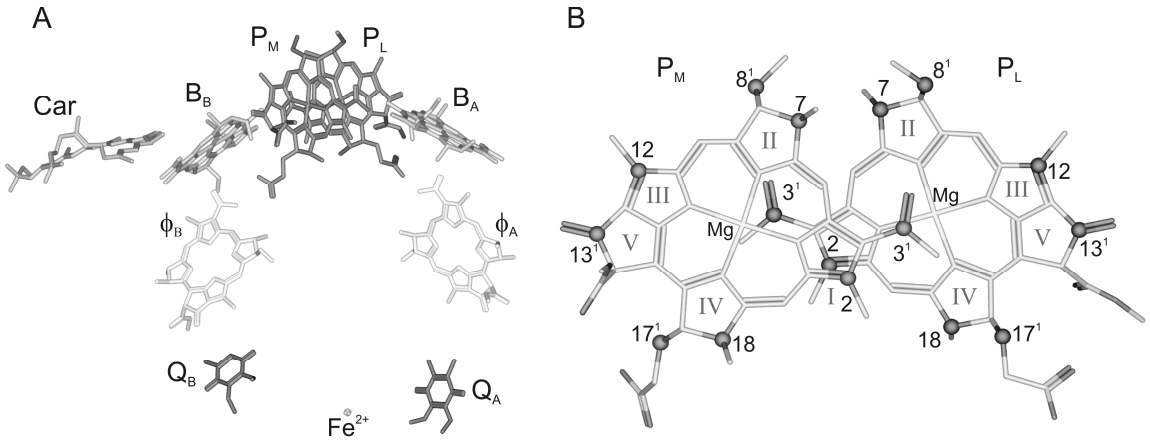

Figure 2.1 (A): Arrangement of cofactors in reaction centers (RCs) of *Rhodobacter (R.) sphaeroides* wildtype (WT). The primary electron donor, the special pair, is formed by the two bacteriochlorophyll *a* (BChl) molecules P_M and P_L. B_A and B_B are accessory BChl cofactors, Φ_A and Φ_B are bacteriopheophytin (BPhe) cofactors. On the acceptor side, two ubiquinone-10 cofactors Q_A and Q_B are located with a non-heme iron in between. The symmetry of the cofactor arrangement is broken by a carotenoid (Car) cofactor. The light-induced electron transfer occurs selectively via branch A. (B): The spatial arrangement of the two cofactors P_L (right, isotope labels in grey) and P_M (left, isotope labels in grey) forming the special pair. The pyrrole rings are numbered with Roman numbers. Pyrrole rings I are overlapping. The isotope labelling pattern has been obtained by feeding with 3-$^{13}C_1$-δ-aminolevulinic acid (3-ALA, see Figure 2.4). The long side chains are omitted to provide a better view on the arrangement of the active elements in the charge separation process. [pdb entry 1M3X, (Camara-Artigas *et al.*, 2002b) the figure has been made with Accelrys Discovery Studio]

al., 2006) and *Rhodopseudomonas acidophila* (Diller *et al.*, 2008), of the green sulphur bacterium *Chlorobium tepidum* (Roy *et al.*, 2007), of the heliobacterium *Heliobacillus mobilis* (Roy *et al.*, 2008) as well as of the photosystems I and II of plants (Matysik *et al.*, 2000a; Alia *et al.*, 2004; Diller *et al.*, 2007b) and algae (Janssen *et al.*, 2010). Hence there is converging evidence that the solid-state photo-CIDNP effect is an intrinsic property of natural photosynthetic RCs (Matysik *et al.*, 2009).

In RCs of *R. sphaeroides*, light absorption induces charge separation within 4 ps from the primary donor (P) to the primary acceptor, a bacteriopheophytin (Φ_A) (for review, see (Hoff & Deisenhofer, 1997)) (Figure 2.1A). The primary electron donor is a special pair formed by 2 bacteriochlorophyll *a* (BChl) cofactors called P_L and P_M (Figure 2.1B). The radical pair is initially in a pure spin-correlated singlet state (Figure 2.2). From this singlet state, photochemically induced dynamic electron polarization (photo-CIDEP) is observed as strongly enhanced absorptive and emissive signals in the EPR spectrum (Blankenship *et al.*, 1975; Hoff *et al.*, 1977). During the lifetime of the radical pair, the electron-spin system oscillates between the singlet ($\underline{S}$) of the radical pair state and the triplet state with magnetic quantum number 0 (T_0), with a frequency that depends on both the hyperfine tensor and the difference of the electron Zeeman interaction between the two electrons forming the radical pair.

The coherent interconversion from singlet to triplet radical pairs and back gives rise to spin sorting within the scheme of the well-known radical pair mechanism (RPM) (Figure 2.2) (Closs & Closs, 1969; Kaptein & Oosterhoff, 1969). Under continuous illumination (CI), the RPM does not induce signal enhancement because the reaction products of both decay branches are identical. Hence, no net nuclear polarization is induced by the RPM in RCs of *R. sphaeroides* WT. Transiently, using time-resolved experiments, however, this nuclear polarization can be observed (Daviso *et al.*, 2009a). Therefore, the sign of the transient light-induced signals follows Kaptein's sign rules (Kaptein, 1971).

In solid-state photo-CIDNP MAS NMR experiments under CI on RCs of *R.*

sphaeroides WT, two additional solid-state mechanisms run in parallel to induce net nuclear polarization which remains under steady-state conditions (Figure 2.2) (Jeschke & Matysik, 2003; Daviso *et al.*, 2008b): (i) Electron–electron–nuclear three-spin mixing (TSM) breaks the balance by coherent evolution of the correlated radical pair state in interaction with the nuclear spins and the applied magnetic field, depending on the signs of the electron–electron and of the anisotropic electron–nuclear interactions (Jeschke, 1997, 1998). (ii) In the electron-nuclear differential decay (DD) mechanism (Polenova & McDermott, 1999), the symmetry is broken by different lifetimes of the S and of the T_0 states. The dependence of

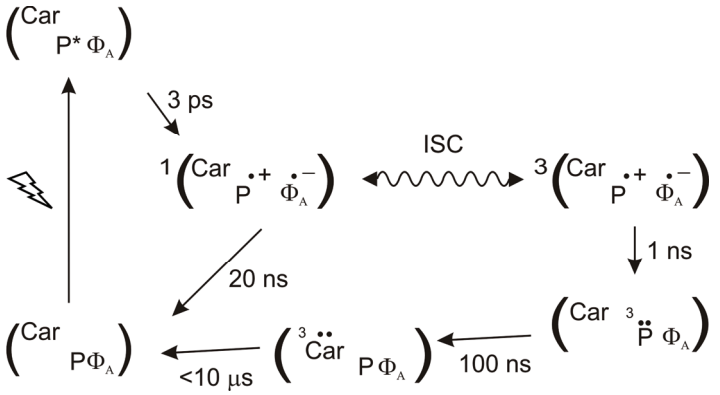

Figure 2.2 Kinetics and spin dynamics of electron transport in quinone-depleted RCs of *R. sphaeroides* wild type (WT). After absorption of a photon the photochemically excited state of the primary donor P* is formed and an electron is transferred to the primary acceptor Φ_A, a bacteriopheophytin cofactor. Initially, the radical pair is in its singlet state $^1(P^{\bullet+}\Phi_A^{\bullet-})$. It evolves into a triplet state $^3(P^{\bullet+}\Phi_A^{\bullet-})$ due to the electronic interactions and hyperfine coupling with nearby nuclei, a process which is known as intersystem crossing (ISC). The radical-pair mechanism (RPM) leads to sorting of nuclear spins via the isotropic hyperfine coupling, but without a net increase of the population difference of the spin up and the spin down nuclear states. In the TSM, hyperfine coupling, nuclear and electronic Zeeman interactions, and anisotropic interactions involving electrons and nuclei lead to symmetry breaking and net nuclear polarization that can be observed both in laser excitation experiments and under steady-state conditions. The lifetime for recombination from the singlet state to the ground state is 20 ns, while charge recombination from the $^3(P^{\bullet+}\Phi_A^{\bullet-})$ radical pair state forms a donor triplet state ^3P with a time constant of 1 ns. With continuous illumination the difference in recombination rates from the singlet and triplet states to the neutral ground state also break the symmetry when they match the inverse of the pseudosecular component of the hyperfine interaction, a process which is known as the DD mechanism. For the WT, the ^3P is rapidly converted (100 ns) in a carotenoid triplet (^{3}Car) and followed by a much slower decay from the carotenoid triplet state to the ground state. Time-resolved experiments have shown that a large fraction of the excited state decays via ^{3}Car, in competition with back conversion to the $^3(P^{\bullet+}\Phi_A^{\bullet-})$ that decays rapidly with 20 ns to establish the steady state. Before reaching this steady state, however, transient effects from RPM, TSM and DD can be observed with time-resolved photo-CIDNP, on a timescale of 10 µs and different mechanisms can be resolved by adjusting the time between the photo-CIDNP excitation and the NMR detection scheme.

secular part of the hyperfine coupling is the only single matching of interactions $2|\omega_I| = |A|$ is required and the difference of singlet and triplet radical pair lifetimes must be of the order of the inverse hyperfine coupling (Jeschke & Matysik, 2003).

In time-resolved experiments on RCs of *R. sphaeroides* WT, transient nuclear polarization has been observed up to 10 μs (Daviso *et al.*, 2009a). The decay from the singlet state to the ground state is 20 ns, much faster than the pathway via the three triplet states, which is rate limited by the decay from the carotenoid triplet state to the ground state, 10 μs (Figure 2.2). Thus, transient nuclear polarization can be observed, originating from the nuclear polarization associated with rapid decay of the $^1(P^{\bullet+}\Phi_A^{\bullet-})$ state while the polarization associated with the decay of the T_0 channel is hidden by dipolar dephasing from the paramagnetic triplet on the carotenoid (^{3}Car) during its lifetime. As a result, the nuclear polarization of the triplet decay channel cannot be detected on the nearby nuclei in experiments with a short delay <10 μs between optical excitation and NMR detection (Figure 2.2) (Daviso *et al.*, 2008b; Daviso *et al.*, 2009a).

Time-resolved photo-CIDNP MAS NMR has also been demonstrated to map the electron spin density on the donor with atomic selectivity since the transient nuclear polarization intensities reflect the local electron spin densities on the donor (Daviso *et al.*, 2009c). Interpretation of one-dimensional envelope of transient nuclear polarization however requires chemical shift assignments, which need to be obtained in separate experiments. Here we show that two-dimensional nanosecond laser-flash photo-CIDNP MAS NMR experiments allow for direct measurement of both chemical shifts and local electron spin densities in a single experiment.

2.2 Methodology

2.2.1 Dipolar assisted rotational resonance (DARR) spectroscopy

To explore connectivities between carbons, ^{13}C-^{13}C homonuclear shift-correlation experiments are necessary. In solid state NMR, different pulse sequences have been developed for use with MAS, such as DRAMA (Tycko & Dabbagh, 1990),

RFDR (Bennett *et al.*, 1992; Bennett *et al.*, 1998) , C7 (Lee *et al.*, 1995), PDSD (Szeverenyi *et al.*, 1982; Grommek *et al.*, 2006) and DARR (Takegoshi *et al.*, 2001). With DARR (Dipolar assisted rotational resonance), In the DARR experiment, nuclear polarization transfer is driven by a spin-diffusion-type mechanism while the heteronuclear (^{1}H-^{13}C) dipolar couplings are re-established by continuous ^{1}H rf irradiation on a rotary resonance condition. The pulse program for a DARR experiment is shown in Figure 2.3A. As in any two-dimensional experiment, there are four periods: i) preparation, ii) evolution, iii) mixing and iv) acquisition. In the preparation period, a standard cross polarization (CP) step is used mainly to enhance the ^{13}C polarization, by factor of ~ 4 by transfer of magnetization from the protons. During the evolution period (t_1) the ^{13}C nuclei precess according to their chemical shift. For a well resolved spectrum, efficient heteronuclear ^{1}H-^{13}C decoupling as TPPM is required during this period. After the evolution period, the magnetization is put along the z-axis with a $\pi/2$ pulse and mixing (t_{mix}) occurs longitudinally with low power irradiation on ^{1}H. The ^{1}H rf field strength is set to the n=1 rotary resonance condition (Nielsen *et al.*, 1992). During the acquisition, TPPM (Bennett *et al.*, 1995) is applied in the ^{1}H channel for optimum decoupling.

^{13}C signal assignments can be obtained by analyzing ^{13}C–^{13}C cross peaks in data sets collected with a short mixing time, where polarization transfer by ^{13}C–^{13}C dipolar interactions occurs mostly within directly bonded ^{13}C–^{13}C pairs. At longer mixing times, long range correlations may also be observed. In broadband dipolar recoupling experiments, however, such long-range correlations are quenched by dipolar truncation (Takegoshi, 2008). The strong dipolar coupling for a pair of adjacent ^{13}C–^{13}C spins tends to obscure weaker couplings between a ^{13}C spin in the pair and remote ^{13}C spins (Baldus & Meier, 1997; Hoshino *et al.*, 1998; Hohwy *et al.*, 1999). However, DARR produces broadband recoupling of weakly interacting ^{13}C spins without appreciable dipolar truncation effects even though the sample is extensively ^{13}C labelled (Takegoshi *et al.*, 2003; Crocker *et al.*, 2004; Igumenova *et al.*, 2004). In addition to broadband recoupling, DARR has other features that

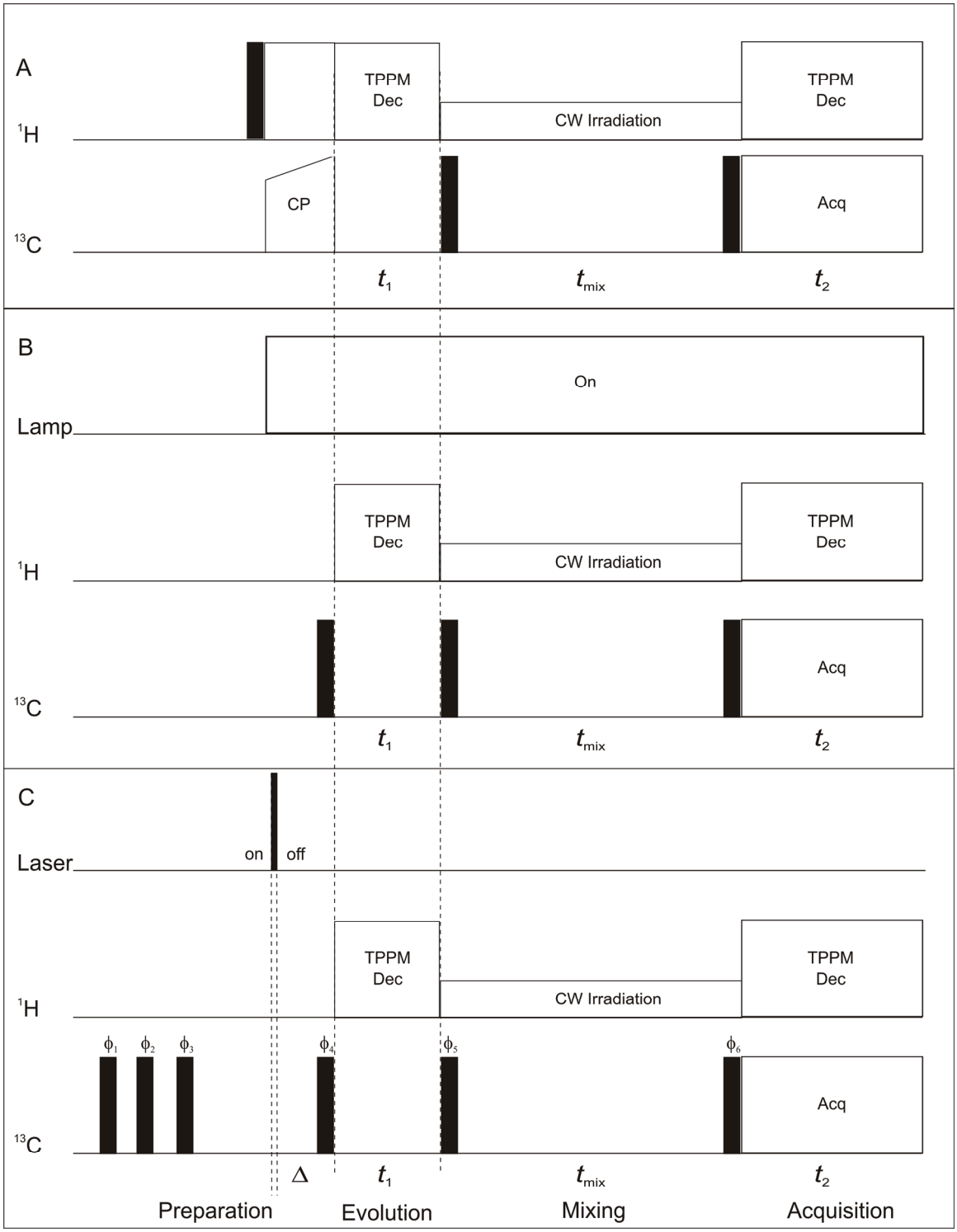

Figure 2.3 Two-dimensional ^{13}C-^{13}C CP DARR MAS NMR pulse program. Solid bars indicate the π/2 pulses and CP is cross polarization, TPPM and CW are different types of decoupling methods that can be applied, while Acq is the acquisition. t_1 and t_2 are the indirect and direct dimensions of the 2D experiment and t_{mix} is the spin diffusion mixing time. (A) Standard DARR experiment, (B) modified DARR experiment with CI setup, (C) Two-dimensional ^{13}C-^{13}C photo-CIDNP laser DARR MAS NMR pulse program used for the experiment. Solid bars indicate the π/2 pulses, Δ is the delay between the laser pulse and the π/2 pulse on the carbon channel, here Δ= 0 μs, during the ^{13}C mixing time ^{1}H was irradiated under the rotational resonance condition ($\omega_{1H} = n\omega_R$). The phase cycling used in the pulse program is Φ_1 = 0 2, Φ_2 = 0, Φ_3 = 2, Φ_4 = 0 0 0 0 0 0 0 0 2 2 2 2 2 2 2 2, Φ_5 = 0 0 0 0 2 2 2 2, Φ_6 = 0 2 1 3 and receiver Φ_R= 0 2 1 3 2 0 3 1 2 0 3 1 0 2 1 3. Here definitions are: 0 = +X, 1 = +Y, 2 = -X, 3 = -Y.

make it very suitable for homonuclear shift-correlation experiments: (i) tolerance with respect to the spinning speed and its stability, (ii) low rf-power requirements, (iii) tolerance to rf inhomogeneity, and (iv) good signal strength when a long mixing time is applied, comparable to the spin-lattice relaxation time of ^{13}C. Finally, cross peak intensities in DARR experiments at lower spinning frequencies correlate well with internuclear distances (Takegoshi *et al.*, 2003).

2.2.2 Modified DARR for photo-CIDNP under continuous illumination

The modified pulse program using the strong initial ^{13}C polarization provided by the solid-state photo-CIDNP effect is displayed in Figure 2.3B. The preparation period has been modified from the standard DARR experiment (Figure 2.3A) by replacing the CP segment with a simple ^{13}C $\pi/2$ pulse. Light is obtained from a 1000-W xenon arc lamp (Matysik *et al.*, 2000b).

2.2.3 Modified DARR for photo-CIDNP under laser-flash illumination

The modified pulse program using the strong initial ^{13}C polarization provided by the solid-state photo-CIDNP effect is displayed in Figure 2.3C. The preparation period has been modified from the standard DARR experiment (Figure 2.3A) by removing the CP segment to enhance the ^{13}C signal. Advanced photo-CIDNP techniques are used here for selective excitation of the source for the nuclear polarization, and the laser-flash photo-CIDNP segment (Daviso *et al.*, 2008a) is incorporated, using a laser flash and a subsequent $\pi/2$ pulse. The presaturation of ^{13}C pulses allows for accelerating the experiment by destroying any residual polarization from the previous $\pi/2$ pulse.

2.3 Materials and Methods

2.3.1 Sample preparation

The selective isotopic labelling in RCs of *R. sphaeroides* is achieved by feeding of selectively labelled 3-$^{13}C_1$-δ-aminolevulinic acid (3-ALA), which is a precursor for the formation of BChl and BPhe (Figure 2.4), and leads to a ^{13}C enrichment of

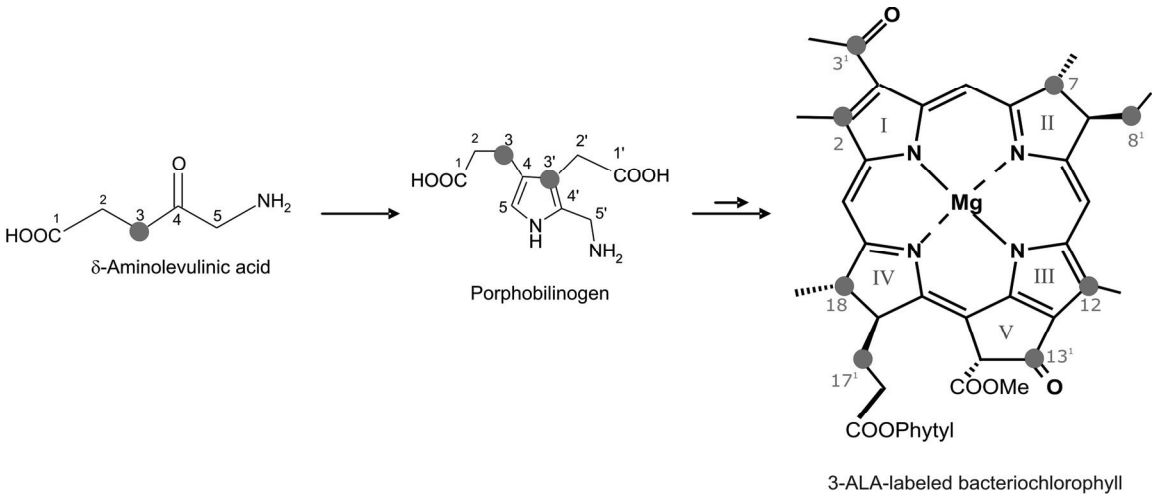

Figure 2.4 Biosynthetic pathway for the formation of selectively ^{13}C isotope labelled bacteriochlorophyll *a* (BChl) by feeding the bacteria with 3-$^{13}C_1$-δ-aminolevulinic acid (3-ALA).

~60% (Schulten *et al.*, 2002). The 3-ALA has been purchased from Buchem B.V. (Apeldoorn, The Netherlands).

The RCs were isolated as described earlier (Shochat *et al.*, 1994) and the quinones were removed by incubating the RCs at a concentration of 0.6 µM in 4% LDAO, 10 mM *o*-phenanthroline, 10 mM Tris buffer, pH 8.0, containing 0.025% LDAO and 1 mM EDTA (Okamura *et al.*, 1975). Approximately 15 mg of RC protein complex embedded in LDAO micelles were used for a NMR experiment.

2.3.2 MAS NMR experiments

NMR experiments were performed with an Avance DMX-200 NMR spectrometer equipped with a double resonance CP/MAS probe (Bruker-Biospin, Karlsruhe, Germany). The sample was loaded into a clear 4-mm sapphire rotor and inserted into the MAS probe. It was frozen slowly at a low spinning frequency of 600 Hz to ensure a homogeneous sample distribution against the rotor wall (Fischer *et al.*, 1992). The light and dark spectra were collected using a Hahn echo pulse sequence with the CYCLOPS phase cycle of the (π/2) pulse. The data were collected with TPPM carbon-proton decoupling (Bennett *et al.*, 1995) at a temperature of 223 K under continuous illumination with white light (Matysik *et al.*, 2001). The optimum length of the (π/2) carbon pulse, determined on uniformly ^{13}C labelled tyrosine, is ~4.0 µs at a strength of 62.5 kHz. The rotational frequency for MAS was

8 kHz. A total number of 128 scans were collected with a recycle delay of 4 s and a line broadening of 10 Hz was applied prior to Fourier transformation. The ^{13}C-MAS NMR spectra were referenced to the ^{13}COOH response of solid tyrosine·(HCl) at 172.1 ppm. All the spectra were phased by using only the zeroth order phase correction.

2.3.3 Lamp set up

The continuous illumination setup for the MAS NMR experiments comprises a 1000-Watt xenon arc lamp with collimation optics, a liquid filter and glass filters, a focusing element and a light fiber. Since the emission spectrum of a Xe lamp is similar to sunlight, the full range of radiation from UV to IR is available for illumination. Disturbance of the spinning frequency counting, which operates from a weak light source in the near-IR region, was avoided by water and also by various glass filters such as W27 and K3G. A fiber bundle was used to transfer the radiation from the collimation optics to the sample (Matysik *et al.*, 2000b; Daviso *et al.*, 2008b).

2.3.4 2D ^{13}C-^{13}C photo-CIDNP DARR MAS NMR under continuous illumination

All the two-dimensional (2D) ^{13}C-^{13}C photo-CIDNP DARR MAS NMR experiments were recorded with a DMX-200 (4.7 Tesla) magnet system. The sample has been frozen in the dark. Samples were kept spinning at 8 kHz at a temperature of 223 K under continuous illumination with white light (Matysik *et al.*, 2000b). The DARR pulse program was modified to incorporate the excitation with light (Figure 2.3B). For DARR experiments, all spectra were collected with 200 t_1 increments and 64 scans, with a recycle delay of 4 s. A spin diffusion mixing time of 1 second was applied.

2.3.5 Laser setup

Using 1064-nm flashes of a Nd:YAG laser (SpectraPhysics Quanta-Ray INDI 40-10, Irvine CA, USA), and frequency-doubling with a second harmonic generator, 532-

nm laser flashes were generated with pulse lengths of 6-8 ns and an energy between 20 to 270 mJ. The laser was operating with repetition rates between 1 and 4 Hz. Time-resolved photo-CIDNP MAS NMR data were acquired with NMR detection immediately after light excitation, using a presaturation pulse sequence to erase the polarization and coherence from previous scans as described in Daviso *et al.* (Daviso *et al.*, 2008a).

2.3.6 2D ^{13}C-^{13}C photo-CIDNP laser DARR MAS NMR experiments

The 2D ^{13}C-^{13}C photo-CIDNP laser-flash DARR MAS NMR experiment was recorded with the sample spinning at 8 kHz at a temperature of 223 K using a DMX-200 (4.7 Tesla) magnet system. The sample was frozen in the dark. The pulse program was modified to incorporate the triggering of the laser pulse CIDNP excitation (Figure 2.3C). For laser-flash DARR experiments, all spectra were collected with 100 t_1 increments in 3024 scans, with a recycle delay of 4 s. A spin diffusion mixing time of 1 second was applied.

2.3.7 Data processing

All spectra were processed using the TopSpin (version 1.2) software package (Bruker-Biospin, Karlsruhe, Germany). The Qsine window function was applied along with zero-filling to 1024 data points in both the t_1 and the t_2 dimensions.

2.4 Results

2.4.1 1D ^{13}C MAS NMR experiments

Figure 2.5 shows the one-dimensional ^{13}C MAS NMR spectra of 3-ALA labelled RCs of *R. sphaeroides* WT. The data were obtained in a magnetic field of 4.7 Tesla and at a temperature of 223 K with a MAS frequency of 8 kHz. Figure 2.6 provides a detailed view on the carbonylic and aliphatic regions.

Spectrum A in Figure 2.5 is collected in the dark, and no signal is observed. Upon CI with white light, strong polarization is established (Spectrum B in Figure 2.5 and 2.6). All signals are light-induced and emissive (negative). The sign of the signal has been explained by the dominance of the TSM over the DD mechanism (Prakash *et al.*, 2005). The two strongest signals at 119.4 and 134.2 ppm have been assigned to the C-12 and C-2 carbons, respectively. The strong solid-state photo-CIDNP effect confirms that these aromatic carbons obtain direct strong enhancement from the electron spin that is delocalized over the special pair (Daviso *et al.*, 2008b). All other signals are considerably weaker. At least four signals can be distinguished in the carbonyl region. The carbonyl carbon atoms are labelled and may gain intensity from the nearby C-2 and C-12 that are strongly polarized. The intensity of the signals in the aliphatic region between 0 and 60 ppm is less than for the signals in the aromatic region. Since for unlabelled RCs

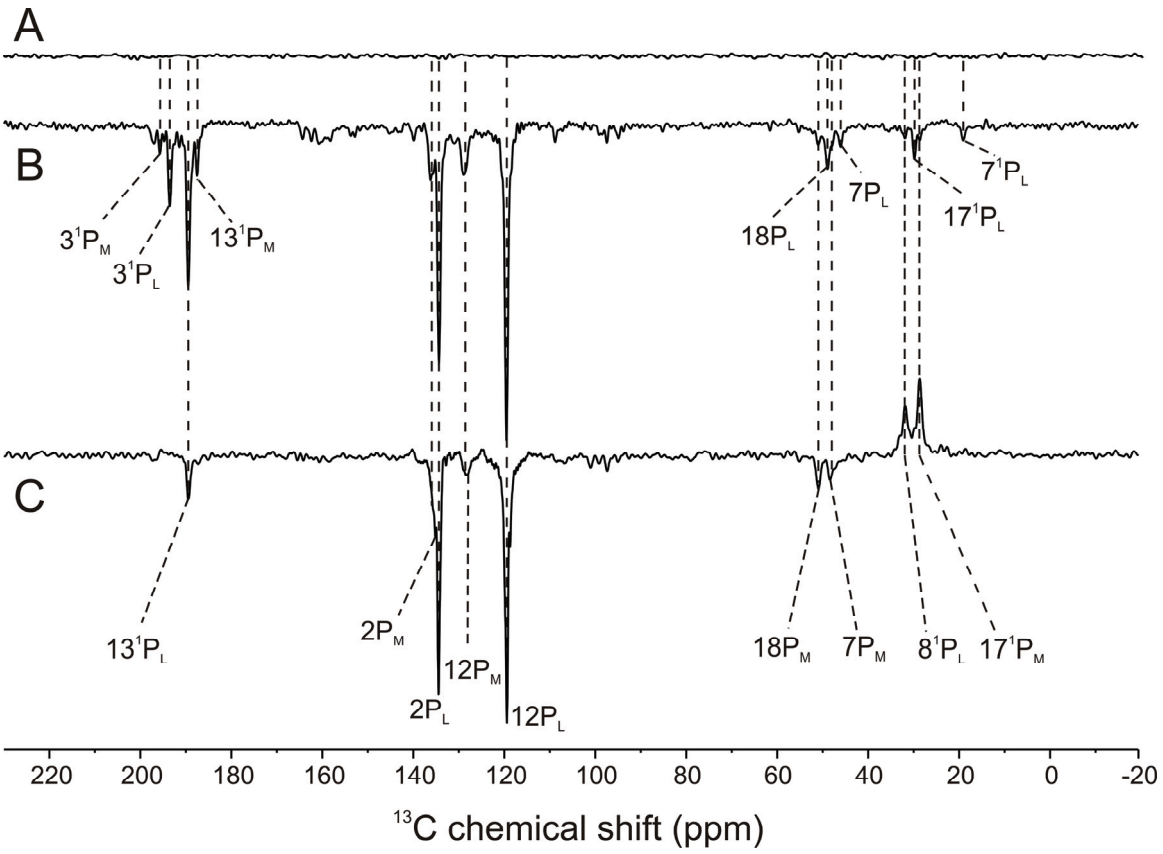

Figure 2.5 One-dimensional ^{13}C photo-CIDNP MAS NMR spectra of 3-ALA labelled RCs of *R. sphaeroides* WT (A) in the dark, (B) under continuous light and (C) under nanosecond laser-flash with $\Delta = 0$ µsec.

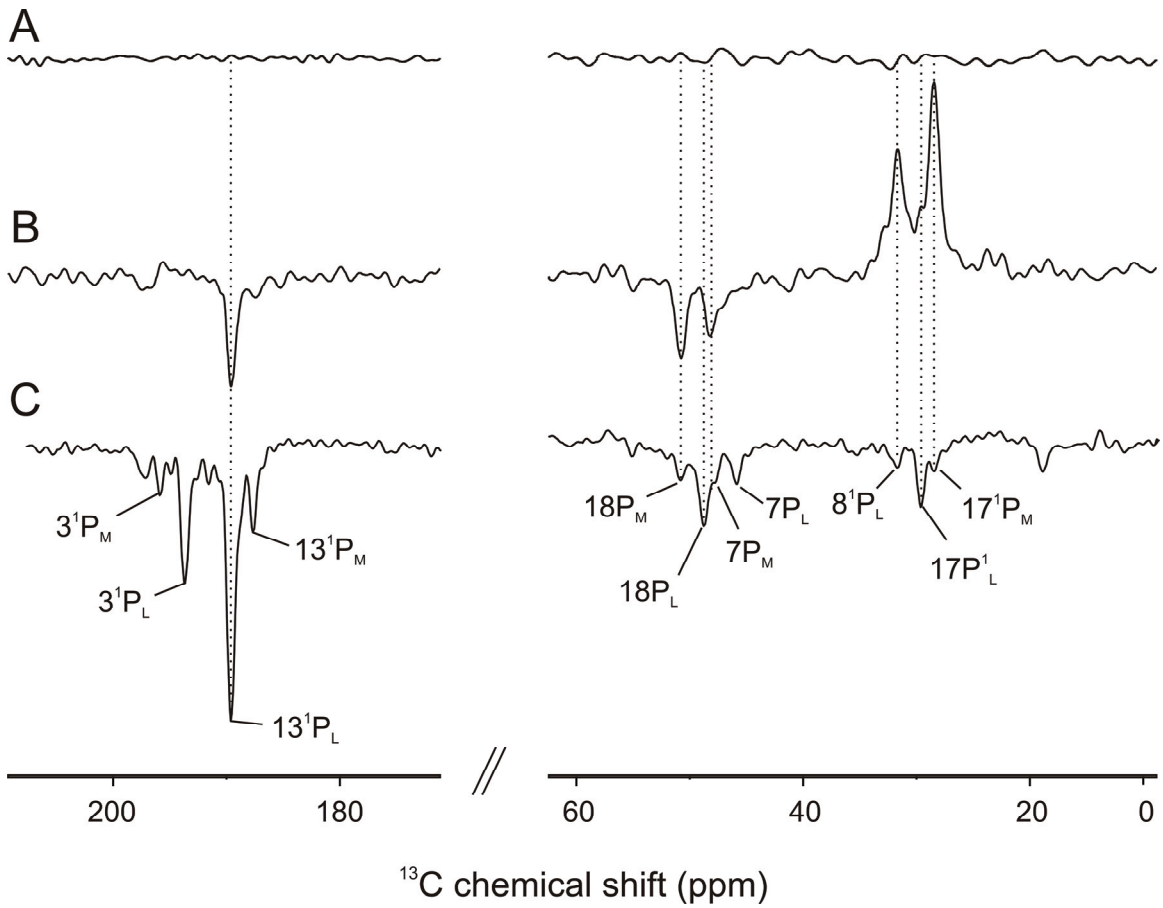

Figure 2.6 Carbonyl and aliphatic regions of one-dimensional ^{13}C photo-CIDNP MAS NMR spectra of 3-ALA labelled RCs of *R. sphaeroides* WT (A) in the dark, (B) under nanosecond laser-flash with Δ = 0 µsec and (C) under continuous light.

under continuous illumination, very little photo-CIDNP arises at aliphatic carbons (Prakash *et al.*, 2005), the observed intensity gain in the 1D experiments is attributed to transfer from strongly polarized aromatic carbons by ^{13}C spin diffusion.

In Spectrum C in Figure 2.5 and 2.6, photo-CIDNP is induced by laser flashes, immediately followed by NMR detection. This spectrum's signs are from the RPM, and the signals are both absorptive and emissive (Kaptein, 1971). As discussed in the above theory section, the sign and intensities of the transient response provides direct access to isotropic hyperfine values.

2.4.2 Continuous illumination 2D ^{13}C-^{13}C photo-CIDNP DARR MAS NMR spectrum

In Figure 2.7A, the two-dimensional ^{13}C-^{13}C photo-CIDNP DARR MAS NMR spectra of 3-ALA labelled RCs of *R. sphaeroides* WT obtained under continuous illumination with white light are shown. The spin-diffusion mixing time is 1 s. In addition to the diagonal peaks, several cross peaks are observed. In such 2D experiments, generally spins are allowed to evolve at their characteristic frequency during the t_1 and t_2 time intervals. During the mixing period (t_{mix}), between t_1 and t_2, magnetization is transferred between spins via the dipolar coupling. In general, spins that are close in space will interact. Thus, a two-dimensional dataset is collected as a function of both t_1 and t_2. Two-dimensional Fourier transformation of this time domain dataset leads to a two-dimensional frequency spectrum, with frequency axes labelled f_1 and f_2, corresponding with the t_1 and t_2 axes in the time domain, respectively. Signals along the $f_1 = f_2$ diagonal are autocorrelation peaks and arise from magnetization that did not transfer between spins during the mixing period. Additionally, there are cross peaks present as a result of transfer of magnetization by the dipolar coupling during the t_{mix} period between the interacting spins. Hence, the intensity and the sign of the cross peaks depends on the state obtained after the preparation, at the start of the evolution period t_1, and reflect the strength and sign of correlated diagonal peaks along the f_2 dimension.

Many carbons of the BChl cofactors of the special pair have been already assigned in previous studies on unlabelled (Prakash *et al.*, 2005; Prakash *et al.*, 2006), 4-ALA (Schulten *et al.*, 2002; Daviso *et al.*, 2009a) and 5-ALA (Prakash *et al.*, 2007) labelled WT RCs. While the 4- and 5-ALA label patterns allow to study the aromatic carbons of the BChl and BPhe macrocycles, 3-ALA labelling leads to isotope enrichment of the more peripheral carbon positions (Figure 2.1 and 2.4). This label pattern is particularly suitable for observation of spin diffusion since it combines a range of internuclear distances for the bacteriochlorin rings and some side chains with a good dispersion of chemical shifts that facilitates the detection of transfer between pairs of labels.

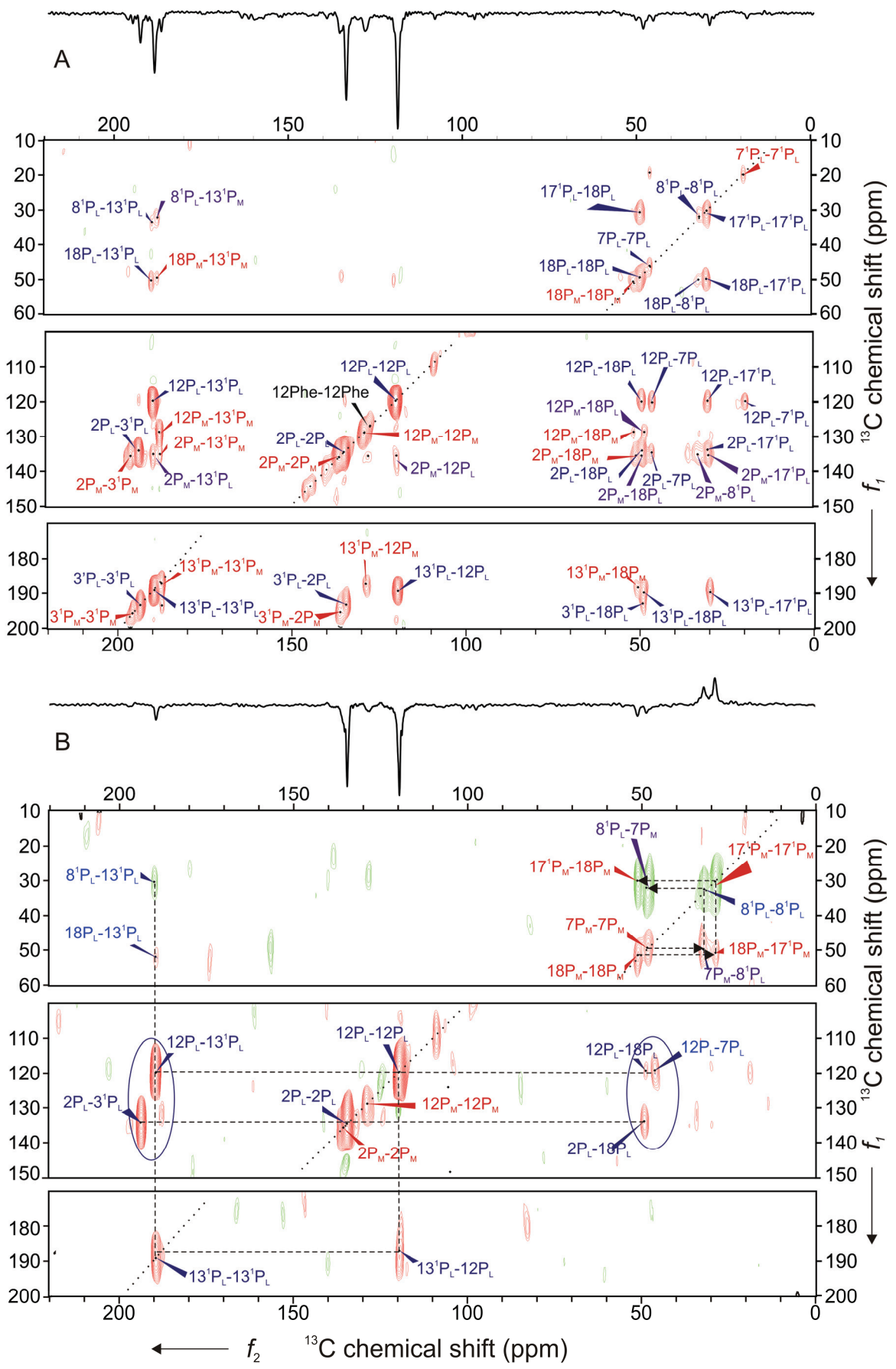

Figure 2.7 Two-dimensional ^{13}C-^{13}C photo-CIDNP DARR MAS NMR spectra of 3-ALA labelled RCs of *R. sphaeroides* WT with a spin-diffusion mixing time of 1 s, collected with a spinning frequency of 8 kHz at a temperature of 223 K. (A) Light source used is a 1000 W xenon lamp. (B) Data obtained with the laser setup. Circled region displayed less number of cross peaks in laser experiment compared to the same regions with CI experiment.

In photo-CIDNP MAS NMR on RCs of *R. sphaeroides* WT, signals from three cofactors are enhanced, the two BChl cofactors of the special pair and the primary electron acceptor BPhe in the active A branch. In the DARR spectrum of Figure 2.7, however, only two networks are observed. The more extended network is labelled in blue and is assigned to cofactor P_L of the special pair. It represents a complete set of correlation signals for eight carbon nuclei, including the responses from the C-2 and the C-12 with the strongest intensities. From this network, all chemical shift assignments have been obtained (Table 2.1). A second network, labelled in red, is from a spin system comprising five ^{13}C nuclei, and is assigned to cofactor P_M. As observed previously, most of the signals assigned to P_L are shielded compared to the signals of P_M (Schulten *et al.*, 2002; Prakash *et al.*, 2005; Prakash *et al.*, 2007; Daviso *et al.*, 2009c). In particular the difference between the chemical shifts of the C-12 atoms of 9.0 ppm is remarkable.

2.4.3 Time-resolved 2D ^{13}C-^{13}C photo-CIDNP DARR MAS NMR spectrum

Figure 2.7B shows the two-dimensional ^{13}C-^{13}C photo-CIDNP laser DARR MAS NMR spectra of 3-ALA labelled RCs of *R. sphaeroides* WT collected at 223 K with a spin-diffusion mixing time of 1 s and a MAS frequency of 8 kHz. In time-resolved experiments on RCs of *R. sphaeroides* WT without a delay between laser flash and NMR detection, the light-induced signals are mainly due to the transient polarization as explained in (Figure 2.2) (Daviso *et al.*, 2009a). Hence, the ^{13}C-^{13}C correlation experiment provides both a view on the electronic structure and the chemical shift assignments of the labelled atoms in the special pair.

In the time-resolved two-dimensional spectrum, mainly peaks from P_L appear and only a few from P_M. In the one-dimensional dataset collected with laser excitation, the signals in the aliphatic region are strong compared to the CI experiment and the signals from C-17^1 P_M, C-17^1 P_L and C-8^1 P_L are absorptive. In Figure 2.7, selected regions of 2D spectra are displayed. Since Figure 2.7A is obtained with CI, all diagonal peaks are emissive, which leads to a completely emissive sets of cross peaks. The cross peak intensities confirm that the signal

Table 2.1 Assignment of the signals from 3-ALA-labelled BRCs obtained with continuous illumination and nanosecond laser-flash excitation, with their respective signs of polarization. For the continuous illumination experiment all the polarization is emissive. (E = emissive; A = absorptive).

Carbon's position in BChl *a*	P_L	Sign in laser expt	P_M	Sign in laser expt	BPhe
2	134.3	E	136.2	E	
3^1	193.5	-	195.6	-	
7	46.1	-	48.3	E	
8^1	32.1	A			
12	119.5	E	128.8	E	126.9
13^1	189.4	E	187.5	-	
17^1	29.9	A	28.4	A	
18	49.1	-	50.9	E	
7^1	19.1	-		-	

strength is transferred along the f_2 dimension. For example, the cross peak, C12 (P_L) / $C7^1$ (P_L) is very pronounced, as the corresponding diagonal peak in the f_2 direction is also strong. In Figure 2.7B, laser flashes were used as source of the photo-CIDNP enhancement and both absorptive and emissive signals occur. The cross peaks in the aliphatic region, for example, C18 (P_M) / $C17^1$ (P_M) show the same sign as the diagonal peaks along the f_2 dimension (see dashed arrows).

Compared to the continuous illumination experiment, less diagonal peaks occur due to the selectivity of the RPM, therefore also less cross peaks are observed for the same mixing time of 1 s. Hence, the enhancement mechanism in the 2D Laser-DARR acts as a filter for correlation experiments. The higher selectivity also allows for clarifying the assignments for C7 (P_M), C7 (P_M), C8 (P_L) and C18 (P_M) (Table 2.1).

2.4.4 Experimental reconstruction of the electronic structures of the Special Pair

Nearly complete sets of ^{13}C assignments for the macrocyles of both the P_L and P_M cofactors are presented in Table 2.2 and 2.3, respectively, compiling the results of this work using the 3-Ala label pattern (Table 2.1) with that of previous work using 4- and 5-Ala label patterns (Schulten *et al.*, 2002; Prakash *et al.*, 2007; Egorova-Zachernyuk *et al.*, 2008; Daviso *et al.*, 2009a). After correction for ring current effects, the comparison of ^{13}C chemical shifts of the special pair with chemical shifts obtained from a BChl in solution in chloroform provide the full signature of the ground state electronic structure with great detail (Figure 2.8). Apparently the formation of the supermolecule leads to a concentration of electronic shielding, indicated with yellow spheres in the overlap region of pyrrole rings I of P_L and P_M (Figure 2.8). These results validate the earlier observations for RCs of the carotenoid-less mutant R26 (Daviso *et al.*, 2009c) and show that the presence of the carotene has little effect on the ground state electronic properties and the structure of the Special Pair. In addition, theoretical studies indicate that accumulation of negative charge on the P_L and P_M can be established by partial charge transfer from the axial histidines HisL173 and HisM202 (Alia *et al.*, 2009; Wawrzyniak *et al.*, 2011).

Figure 2.8 compiles the differences in chemical shift, reflecting the shielding and deshielding by the electronic distribution for the ground state of the Special Pair. This has been experimentally obtained in the present study by the laser-flash experiment (Table 2.1). In line with earlier time-resolved photo-CIDNP studies, the P_L is more shielded than the P_M (Zysmilich & McDermott, 1994; Schulten *et al.*, 2002; Prakash *et al.*, 2007; Daviso *et al.*, 2009c). For both cofactors, considerable shielding is observed for the ^{13}C on pyrrole rings I, indicating accumulation of electron density in the overlap region. The shift pattern also points to more relative electron density on the pyrrole ring III of P_L , while the pyrrole ring III of P_M is deshielded, indicating accumulation of positive charge in the region.

Table 2.2 ^{13}C positions in P_L and their NMR chemical shifts [1].

Carbon's position in BChl *a*	Chemical shift (ppm) of BChl *a* in acetone solution [a]	Chemical shift (ppm) of P_L			
		Measured by MAS NMR	Calculated ring current	Real CS Corrected (observed -calculated ring current)	Corrected (corr CS-CS in liquid)
	δ_{Model}	δ_{PL}	δ_{RC}	$\delta_{PL(Corr)}= \delta_{PL}- \delta_{RC}$	$\Delta_{(Corr)}= \delta_{PL(Corr)}- \delta_{Model}$
1	151.2	143.5 [b]	-1.3	144.8	-6.4
2	142.0	134.3 [c]	-2.3	136.6	-5.4
3	137.7	127.4 [b]	-3.3	130.7	-7.0
3[1]	199.3	193.5 [c]	-4.2	197.7	-1.6
4	150.0	136.8 [b]	-2.0	138.8	-11.2
5	99.9	103.0 [b]	-1.1	104.1	4.2
6	168.9	165.9 [b]	-0.1	166.0	-2.9
7	48.3	46.1 [c]	0.3	45.8	-2.5
7[1]	23.4	19.1 [c]	0.0	19.1	-4.3
8	55.8	54.7 [b]	0.2	54.5	-1.3
8[1]	30.8	32.1 [c]	0.4	31.7	0.9
9	158.5	162.6 [b]	0.2	162.4	3.9
10	102.4	100.4 [b]	0.2	100.2	-2.2
11	149.5	153.6 [b]	0.2	153.4	3.9
12	124.0	119.5 [c]	0.2	119.3	-4.7
13	130.6	130.8 [b]	0.2	130.6	0.0
13[1]	189.0	189.4 [c]	0.2	189.2	0.2
14	160.8	157.2 [b]	0.2	157.0	-3.8
15	109.7	108.7 [b]	0.2	108.5	-1.2
16	152.0	145.6 [b]	0.2	145.4	-6.6
17	50.5	50.0 [b]	0.2	49.8	-0.7
17[1]	30.5	29.9 [c]	0.3	29.6	-0.9
18	49.5	49.1 [c]	0.1	49.0	-0.5
19	167.3	161.0 [b]	-0.1	161.1	-6.2
20	96.3	104.1 [b]	-0.5	104.6	8.3

[a] Egorova-Zachernyuk (2008); ([b]) earlier works; ([c]) This work

[1] NMR chemical shifts of P_L (δ_{PL}) , its monomeric chlorophyll in acetone (δ_{Model}) and respective differences in chemical shift after the subtraction of estimated ring current effects ($\Delta_{(Corr)}$).

Table 2.3 ^{13}C positions in P_M and NMR chemical shifts [2].

Carbon's position in BChl *a*	Chemical shift (ppm) of BChl *a* in acetone solution [a]	Chemical shift (ppm) of P_M			
		Measured by MAS NMR	Calculated ring current	Real CS Corrected (observed - calculated ring current)	Corrected (corr CS-CS in liquid)
	δ_{Model}	δ_{PM}	δ_{RC}	$\delta_{PM(Corr)}= \delta_{PM}- \delta_{RC}$	$\Delta_{(Corr)}= \delta_{PM(Corr)} - \delta_{Model}$
1	151.2	148.5 [b]	-1.1	149.6	-1.6
2	142.0	136.2 [c]	-2.1	138.3	-3.7
3	137.7	129.7 [b]	-3.2	132.9	-4.8
3^1	199.3	195.6 [c]	-4.2	199.8	0.5
4	150.0	144.5 [b]	0.1	144.4	-5.6
5	99.9	101.2 [b]	-1.3	102.5	2.6
6	168.9	166.5 [b]	-0.2	166.7	-2.2
7	48.3	48.3 [c]	0.2	48.1	-0.2
7^1	23.4	22.6 [b]	-0.1	22.7	-0.7
8	55.8	52.7 [b]	0.3	52.4	-3.4
8^1	30.8	29.5 [b]	0.6	28.9	-1.9
9	158.5	158.5 [b]	0.3	158.2	-0.3
10	102.4	98.3 [b]	0.1	98.2	-4.2
11	149.5	149.8 [b]	0.3	149.5	0.0
12	124.0	128.8 [c]	0.2	128.6	4.6
13	130.6	132.8 [b]	0.1	132.7	2.1
13^1	189.0	187.5 [c]	0.1	187.4	-1.6
14	160.8	160.1 [b]	0.1	160.0	-0.8
15	109.7	106.6 [b]	0.1	106.5	-3.2
16	152.0	151.5 [b]	0.1	151.4	-0.6
17	50.5	47.4 [b]	0.1	47.3	-3.2
17^1	30.5	28.4 [c]	0.1	28.3	-2.2
18	49.5	50.9 [c]	0.1	50.8	1.3
19	167.3	164.4 [b]	0.0	164.4	-2.9
20	96.3	102.0 [b]	-0.3	102.3	6.0

[a] Egorova-Zachernyuk (2008); ([b]) earlier works; ([c]) This work

[2] NMR chemical shifts of P_M (δ_{PM}) , its monomeric chlorophyll in acetone (δ_{Model}) and respective differences in chemical shift after the subtraction of estimated ring current effects ($\Delta_{(Corr)}$).

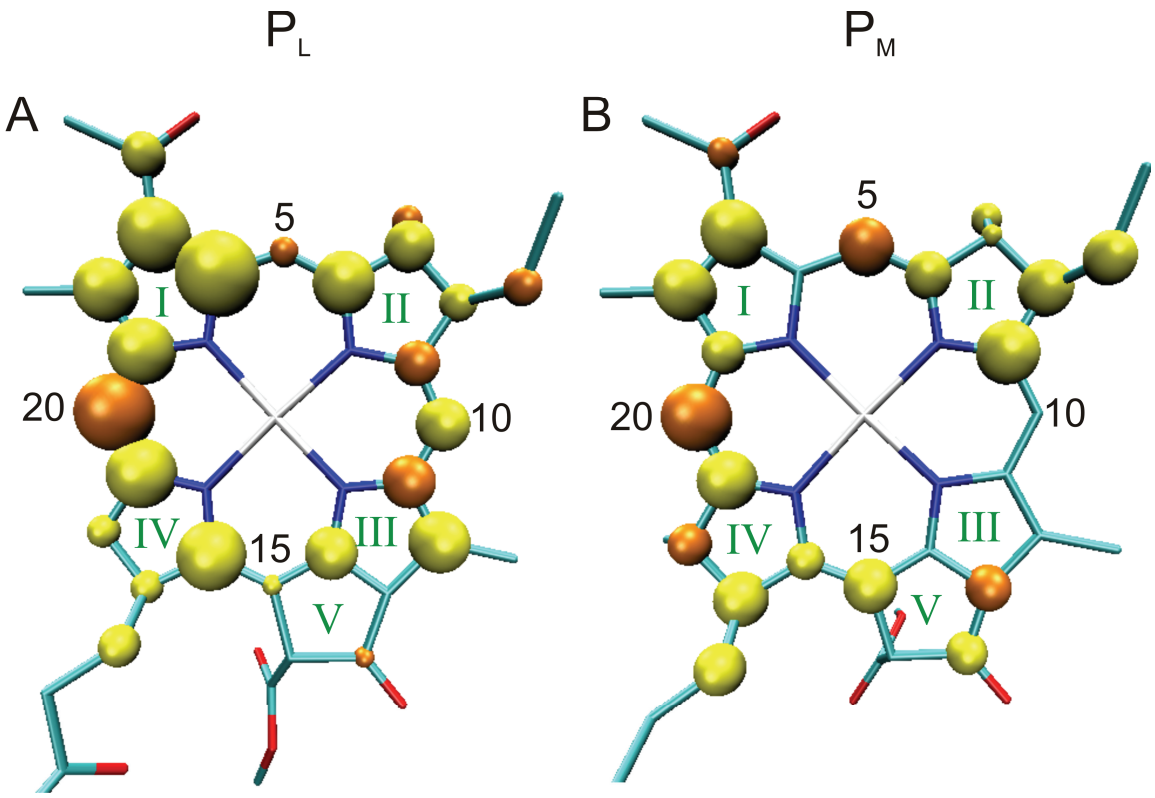

Figure 2.8 The cofactors P_L and P_M of the Special Pair, with the numbering of pyrrole rings and meso carbon atoms. The spheres correspond with the difference in chemical shifts after the correction by the estimated ring current effects, which reflect the relative electronic distribution for P_L and P_M in the electronic ground state derived experimentally. Yellow and orange colored spheres represent negative (shielding) and positive (deshielding) differences in chemical shifts, respectively.

This character of the special pair could be well represented as $P_L^{\delta-}P_M^{\varepsilon-}$, from the photo-CIDNP analysis of the ground state chemical shifts. We find $\delta > \varepsilon$ which would imply that there is some dipole character in the ground state, superimposed on a overall negative charge and is well in line with earlier NMR studies that indicate balancing of the special pair charge state by the protein surroundings (Alia *et al.*, 2009). The electronically excited state and the radical cation state have been studied by other spectroscopic methods. From the absorption and Stark spectroscopy, it has been concluded that the excited state has $P_L^+P_M^-$ charge transfer character, while the radical cation state has more negative charge on the P_L, which parallels the findings in this chapter (Lendzian *et al.*, 1993; Daviso *et al.*, 2009c). The $P_L^{\delta-}P_M^{\varepsilon-}$ charge transfer character and associated symmetry breaking of the electronic structure can possibly mediate asymmetric electron transfer following excitation, which will be further explored in chapter 3.